Multidomains made of different structural phases in multiferroic $BiFeO_3$: A first-principles-based study

Dawei Wang,[1,*] Ekhard K. H. Salje,[2] Shao-Bo Mi,[1,3] Chun-Lin Jia,[1,4] and L. Bellaiche[5]

[1]*Electronic Materials Research Laboratory–Key Laboratory of the Ministry of Education and International Center for Dielectric Research, Xi'an Jiaotong University, Xi'an 710049, China*

[2]*Department of Earth Sciences, University of Cambridge, Cambridge CB2 3EQ, United Kingdom*

[3]*Institute of Metal Research, Chinese Academy of Sciences, Shenyang 110016, China*

[4]*Peter Grünberg Institute and Ernst Ruska Center for Microscopy and Spectroscopy with Electrons, Forschungszentrum Jülich, D-52425 Jülich, Germany*

[5]*Physics Department and Institute for Nanoscience and Engineering, University of Arkansas, Fayetteville, Arkansas 72701, USA*

(Received 9 March 2013; revised manuscript received 21 August 2013; published 21 October 2013)

An effective Hamiltonian scheme is used to reveal the properties of a multidomain structure in $BiFeO_3$ consisting of alternating domains that are initially made of two phases, namely, $R3c$ (ferroelectric with antiphase oxygen octahedral tilting) versus $Pnma$ (antiferroelectric with in-phase and antiphase oxygen octahedral tiltings). These two types of domains dramatically modify their properties as a result of their cohabitation. The weak ferromagnetic vector and polarization rotate, and significantly change their magnitude, in the $R3c$-like region, while the $Pnma$-like region becomes polar along the direction of domain propagation. Moreover, the domain *walls* possess distinct polar and oxygen octahedral tilting patterns that facilitate the transition between these two regions. The studied multidomain is also predicted to exhibit other anomalous properties, such as its strain adopting several plateaus and steps when increasing the magnitude of an applied electric field.

DOI: 10.1103/PhysRevB.88.134107 PACS number(s): 77.80.Dj, 75.60.Ch, 77.55.Nv, 77.84.−s

I. INTRODUCTION

Domains are known to occur in many kinds of materials, including ferroelectrics (FEs), magnets, and ferroelastic compounds.[1–3] They can significantly affect the properties of these systems and even give rise to phenomena that do not occur in the corresponding monodomain. Examples include electronic transport in some energy window[4,5] and above-band gap photovoltaic properties.[6,7] Other examples are superconductivity in the domain walls inside a nonsuperconducting matrix[3] and ferrielectric domain walls in paraelectric $CaTiO_3$.[8–11] The latter examples are representative of a major new research field which was coined domain boundary engineering.[12] An intensive research activity has been devoted to the study of multidomains for which the adjacent domains have the *same* crystallographic phase. Examples are the 71°, 109°, and 180° domains in $BiFeO_3$ (BFO), for which each domain adopts the $R3c$ space group but in which the polarization changes its direction from [111] to [11$\bar{1}$], [1$\bar{1}\bar{1}$], or [$\bar{1}\bar{1}\bar{1}$], respectively, when going from one domain to the adjacent one (see, e.g., Ref. 13 and references therein). Much less investigation has been done on multidomains for which the phases of two adjacent domains are crystallographically different, which is possible because of polymorphism, despite two important facts. (i) Such multidomains can naturally exist if, for example, the material has different, low-energy metastable states and that a first-order transition (which is, e.g., driven by strain or temperature) occurs between these two states. Recent studies[14–16] observed, in highly strained BFO films, nanoscale domains made of the so-called T phase alternating with nanoscale domains formed by the so-called R phase (note that the T phase has a large polarization along the [001] pseudocubic direction, small antiphase oxygen octahedra tiltings, and an unusually high c/a axial ratio, of the order of 1.25, while the R phase possesses a polarization that is smaller and lies close to the [111] direction, as well as much larger antiphase oxygen octahedral tiltings and a much lower c/a, of the order of 1.05). (ii) This type of multidomain is technologically promising and fundamentally intriguing, as evidenced by the reported large piezoelectric response in Ref. 17 and its proposed use in nonvolatile random access memories[18] and as also evidenced by the unusual gradual evolution (over a 20-unit cell length) of the c/a ratio from the unusually high to a much lower value in the domain walls bridging the T and R domains.[14]

It is therefore legitimate to wonder what happens if the two domains are composed of states that are even more different than the T and R phases. A specific example is as follows: the first phase is FE and possesses one type of oxygen octahedral tilting, while the other phase is antiferroelectric (AFE) and exhibits another kind of oxygen octahedral pattern, *and* the magnetization is different in orientation and magnitude between the two phases. Will these two states rearrange their structural and magnetic properties in response to their cohabitation in the multidomain? What kind of domain walls will arise from this coexistence? Will novel physical phenomena emerge in these kinds of multidomain?

Here, we choose to investigate, in BFO, a multidomain formed by domains made by the FE $R3c$ state alternating with domains made by the AFE $Pnma$ phase. These two states are both low-energy phases of BFO systems[19] and it is commonly assumed that $R3c$ transforms into $Pnma$, via a first-order transition, as the temperature increases in BFO bulk.[20] As we see, surprises are in store when investigating this multidomain.

This paper is organized as follows. In Sec. II, we provide details about the numerical technique used in this work. In Sec. III, we present and discuss the results on the BFO multidomain. Finally, in Sec. IV, we briefly summarize this work.

TABLE I. Averaged physical quantities in the pure $R3c$ and $Pnma$ states, as well as in the relaxed $R3c$ and $Pnma$ regions of the studied multidomain configuration. The $\langle \boldsymbol{u}_\Gamma \rangle$ and $\langle \boldsymbol{u}_X \rangle$ vectors are given in arbitrary units; both $\langle \boldsymbol{\omega}_R \rangle$ and $\langle \boldsymbol{\omega}_M \rangle$, as radians. The ferromagnetic moment, $\langle \boldsymbol{m} \rangle$, is given in Bohr magnetons. All these vectors are provided here in a Cartesian setting, with the x, y, and z axes lying along the [100], [010], and [001] pseudocubic directions, respectively.

Physical quantity	Pure $R3c$ state	Relaxed $R3c$ region	Pure $Pnma$ state	Relaxed $Pnma$ region
$\langle \boldsymbol{u}_\Gamma \rangle$	(0.065,0.065,0.065)	(0.040,0.057,0.057)	(0,0,0)	(0.027, − 0.004, − 0.004)
$\langle \boldsymbol{u}_X \rangle$	(0,0,0)	(0, − 0.005, − 0.005)	(0,0.046,0.046)	(0.004,0.031,0.031)
$\langle \boldsymbol{\omega}_R \rangle$	(0.142,0.142,0.142)	(0.116,0.153,0.153)	(0,0.166,0.166)	(−0.009,0.162,0.162)
$\langle \boldsymbol{\omega}_M \rangle$	(0,0,0)	(0.018,0,0)	(0.149,0,0)	(0.082,0,0)
$\langle \boldsymbol{m} \rangle$	(0.02, − 0.01, − 0.01)	(0.03, − 0.01, − 0.01)	(0.04,0,0)	(0.04,0,0)

II. NUMERICAL TECHNIQUE

We use the effective Hamiltonian (Heff) of Ref. 21. Its degrees of freedom are as follows.

(1) The local soft mode in unit cell i, $\boldsymbol{u}_i$, which is directly proportional to the electrical dipole centered on that site. These local modes are centered on Bi sites in this Heff, in order to reproduce the antiferroelectricity associated with some phases of BFO[19,22]—unlike previous approaches.[23–25]

(2) The homogeneous and inhomogeneous strain tensors.[26]

(3) The pseudovectors, $\{\boldsymbol{\omega}_i\}$, which characterize the oxygen octahedra tilting in the unit cells i. $\boldsymbol{\omega}_i$ is centered at the Fe site i and is defined such that its direction provides the axis about which the oxygen octahedra tilt, while its magnitude gives the tilt angle.[27] For instance, $\boldsymbol{\omega}_i = 0.1(\hat{\boldsymbol{x}} + \hat{\boldsymbol{y}} + \hat{\boldsymbol{z}})$ corresponds to a rotation of the oxygen octahedra located at cell i by $0.1\sqrt{3}$ radians about the [111] direction, when denoting by $\hat{\boldsymbol{x}}$, $\hat{\boldsymbol{y}}$, and $\hat{\boldsymbol{z}}$ the unit vectors along the [100], [010], and [001] pseudocubic directions, respectively.

(4) The *magnetic* dipole moments, m_i, centered on the Fe sites (and that are all assumed to have a fixed magnitude or 4-Bohr magneton, as consistent with first-principles computations.)[28]

The parameters of this Heff are determined by performing first-principles calculations on relatively small supercells. More details about this Heff are given in Ref. 21. Its typical outputs, when used within Monte Carlo (MC) simulations on large supercells, are as follows: (i) the $\langle \boldsymbol{u}_\Gamma \rangle$ supercell average of the local mode vectors $\{\boldsymbol{u}_i\}$, which is directly proportional to the electrical polarization; (ii) the $\langle \boldsymbol{\omega}_R \rangle$ vector, which represents antiphase tilting of the oxygen octahedra and is defined as $\langle \boldsymbol{\omega}_R \rangle = \frac{1}{N}\sum_i \boldsymbol{\omega}_i(-1)^{n_x(i)+n_y(i)+n_z(i)}$ [the latter sum runs over the N sites i, and $n_x(i)$, $n_y(i)$, and $n_z(i)$ are integers locating the Fe site i at $a_{\text{lat}}(n_x(i)\hat{\boldsymbol{x}} + n_y(i)\hat{\boldsymbol{y}} + n_z(i)\hat{\boldsymbol{z}}$ with respect to a chosen origin and with a_{lat} being the five-atom cubic lattice constant];[27] (iii) the $\langle \boldsymbol{u}_X \rangle$ vector, which characterizes antiferroelectricity at the X point and which is given by $\langle \boldsymbol{u}_X \rangle = \frac{1}{N}\sum_i \boldsymbol{u}_i(-1)^{n_x(i)}$; (iv) the $\langle \boldsymbol{\omega}_M \rangle$ vector, which quantifies in-phase oxygen octahedral tilting and is provided by $\langle \boldsymbol{\omega}_M \rangle = \frac{1}{N}\sum_i \boldsymbol{\omega}_i(-1)^{n_y(i)+n_z(i)}$; (v) the G-type antiferromagnetic vector $\langle \boldsymbol{L} \rangle$ vector, which is computed as $\langle \boldsymbol{L} \rangle = \frac{1}{N}\sum_i \boldsymbol{m}_i(-1)^{n_x(i)+n_y(i)+n_z(i)}$; and (vi) the ferromagnetic (FM) moment, $\langle \boldsymbol{m} \rangle$, which is the supercell average of the $\{\boldsymbol{m}_i\}$ local magnetic dipoles.

III. RESULTS

This Heff results in the following phase transition sequence: $R3c$–nanoscale twinned phases–$Pnma$–$Pm\bar{3}m$, as the temperature increases from 0 to 1400 K in BFO bulk.[21] It also yields a (meta)stable $Pnma$ state having an internal energy about 70 meV/5 atoms higher than the energy of the $R3c$ ground state at low temperature. Table I reports characteristics of these $R3c$ and $Pnma$ phases at 10 K (they are denoted the "pure $R3c$ state" and "pure $Pnma$ state" in the table). The $R3c$ phase is characterized by a polarization lying along the [111] direction and by antiphase oxygen octahedra tilting about this [111] direction by about 14°, in agreement with the literature.[19,28–32] On the other hand, and consistent with Ref. 19, the $Pnma$ phase has (i) no polarization; (ii) AFE displacements that consist of Bi displacements being oriented along [011] and then [$0\bar{1}\bar{1}$] when going from one to the next (100) Bi-O plane (cf. $\langle \boldsymbol{u}_X \rangle$); (iii) antiphase oxygen octahedra tilting about [011] (cf.$\langle \boldsymbol{\omega}_R \rangle$); and (iv) in-phase oxygen octahedra tilting about [100] (see $\langle \boldsymbol{\omega}_M \rangle$).

We now initially construct a $20 \times 20 \times 20$ supercell (40 000 atoms) that is periodic along all three Cartesian directions and for which the left-half side (along the x axis) is made of this $Pnma$ state and the right-half side (along the x axis) consists of the aforementioned $R3c$ ground state. The resulting domains therefore have an initial size of about 4 nm, which is of the same order as those experimentally found in, e.g., Ref. 33. The electric dipolar configuration and oxygen octahedra tilting patterns in the (x,z) plane of the (unrelaxed) multidomain structure are shown on the left side in Figs. 1(a) and 1(b), respectively. The energy of this unrelaxed multidomain is higher by 210 meV/5 atoms than the pure $R3c$ state and by 139 meV/5 atoms from the pure $Pnma$ phase. This relatively high energy is a manifestation that $R3c$ and $Pnma$ are very different from a crystallographic point of view. For instance, in the initial multidomain configuration, there is a sudden change of the x component of the polarization when going from the nominal paraelectric $Pnma$ region to the domain made of FE $R3c$. This change is not energetically favorable since it goes against the conventional feature that the normal component of the polarization across the domain wall should be conserved.[34]

The multidomain configuration therefore needs to rearrange itself to avoid energy penalties. This rearrangement is observed in our MC simulations (which run over 320 000 sweeps and use the Metropolis algorithm) conducted at 10 K. The resulting patterns of the electric dipoles and oxygen octahedra tiltings in the (x,z) plane in the relaxed structure is displayed on the right side in Figs. 1(a) and 1(b), respectively. Relaxing this multidomain leads to a considerable decrease in its internal energy, by about 150 meV/5 atoms. As a result, the relaxed multidomain possesses an energy that is still (slightly) higher

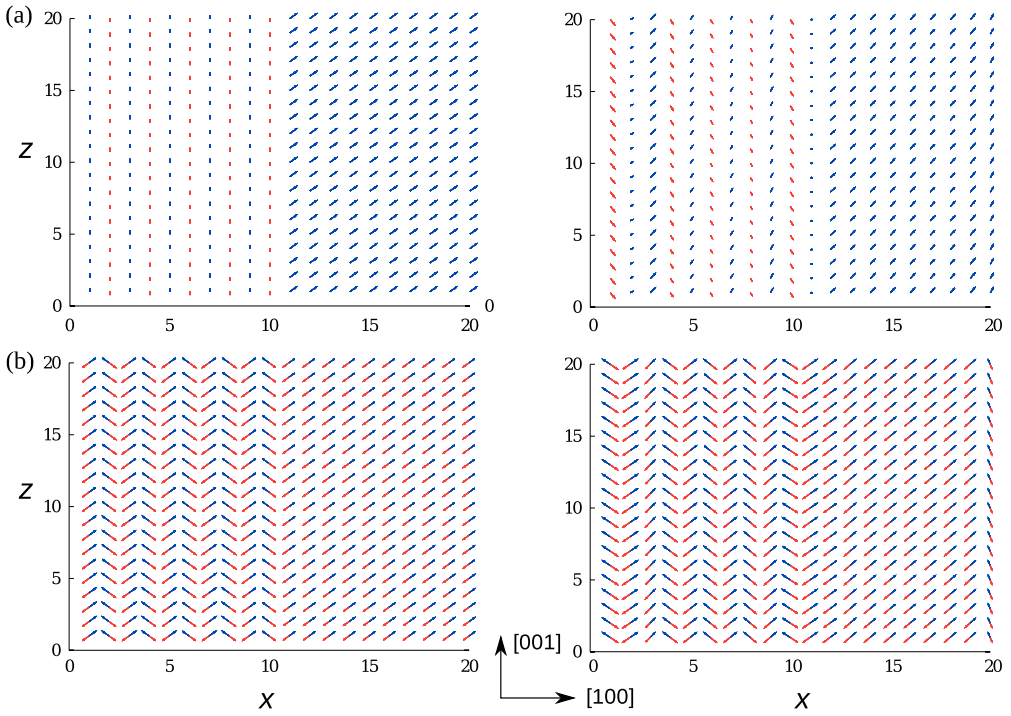

FIG. 1. (Color online) Electric dipolar configuration (a) and oxygen octahedral tilting patterns (b) in the (x,z) plane of the artificially designed multidomain structure before (left column) and after (right column) relaxation.

than that of the pure $R3c$ phase by 60 meV/5 atoms but that is now lower than the energy of the pure $Pnma$ state by $\simeq$11 meV/5 atoms.

Note that our numerical Heff technique naturally includes the internal depolarizing electric field arising from the inhomogeneously distributed polarization inside the multidomain since this method incorporates dipole-dipole interactions, and as shown in Ref. 40, the depolarizing electric field can be computed on the basis of dipole-dipole interactions. A proof of such incorporation in the simulations is our numerical finding that the unrelaxed $R3c/Pnma$ multidomain has a dipole-dipole energy of about 101 meV higher than that resulting from the average between the dipole-dipole energies of the pure $Pnma$ and $R3c$ states (the relaxed $R3c/Pnma$ multidomain has a dipole-dipole energy that is about 32 meV higher than this average). This increase in energy is due to the depolarizing field. Note also that the density of interfaces between $Pnma$ and $R3c$ can affect the energy of this type of multidomain configuration. For example, in another simulation, we generated a system (still using a $20 \times 20 \times 20$ supercell) for which the initial $R3c$ and $Pnma$ domains both have a width of 5 unit cells along x (rather than 10). This new relaxed multidomain configuration has a higher energy (which is still lower than that of the pure $Pnma$ state), while other physical features were noticed to be similar to those of the multidomain structure shown in Fig. 1. We also studied domains having a width of 20 unit cells along x (via the use of a $40 \times 10 \times 10$ supercell), which also confirmed these findings: the lower the density of interface (or, equivalently, the larger the $R3c$ and $Pnma$ domains), the lower the total energy of the relaxed multidomain, while effects reported and discussed in the present work are qualitatively unaffected by this density. Note also that the temperature is purposely chosen to be 10 K here, because the associated thermal energy is lower than the different energetic barriers separating the $R3c$, $Pnma$, and nanoscale twinned phase found in Ref. 21. As a result, the whole system cannot transform to any of these pure phases (which are all stable) and therefore remains in a multidomain configuration. Finally, let us point out that we also constructed another multidomain that fully satisfies the continuity of the normal component of the polarization across the domain wall. This multidomain is composed of $Pnma$ and $R3c$ regions that alternate along the [1-10] direction, and where the $R3c$ region has FE-related dipoles lying along [111], while the $Pnma$ region possesses AFE-related dipoles that are oriented along the [110] or [-1-10] pseudocubic directions. In this multidomain, the direction of alternation of the $R3c$ and $Pnma$ regions cannot therefore coincide with the axis of the in-phase oxygen octahedral tilting occurring in the $Pnma$ phase, unlike in the multidomain we consider in the present work. Interestingly, this domain (for which the normal component of the polarization is conserved across the domain wall) does not survive the MC relaxation procedure but, rather, transforms into a pure $R3c$ state during this relaxation. These facts are consistent with an important finding of Refs. 13 and 35, namely, that the accommodation of antiferrodistortive motions across the domain walls is an important aspect of low-energy multidomains in BFO.

Table I reports some averaged characteristics of the multidomain depicted in Figs. 1(a) and 1(b) in its relaxed $R3c$ and $Pnma$ regions. Note that the relaxed $R3c$ region contains the 10 (100) BiO layers located at the right x side of the supercell (for computing properties related to local modes) and the 10 (100) FeO_2 layers placed at the right side of the supercell along the x axis (for evaluating properties related to oxygen octahedral tiltings and magnetism). Conversely, the

relaxed *Pnma* region elongates over the 10 (100) BiO layers and 10 (100) FeO_2 layers at the left side of the supercell. Important information revealed by Table I is that the modified *R*3*c* region has significantly decreased both the *x* component of its polarization and the *x* component of its antiphase oxygen octahedra tilting (while increasing the *y* and *z* components of $\langle \boldsymbol{\omega}_R \rangle$) with respect to the nominal, pure *R*3*c* phase. It has also acquired a rather small in-phase oxygen octahedra tilting about the *x* direction and a tiny $\langle \boldsymbol{u}_X \rangle$ AEF vector. The modified *Pnma* region also readapts itself by becoming *polar*—that is, by acquiring a significant polarization that mostly lies along the *x* axis—and by now exhibiting a small *x* component of $\langle \boldsymbol{\omega}_R \rangle$. This modified *Pnma* region also possesses an AFE vector and an in-phase oxygen octahedra tilting that have both considerably decreased in magnitude with respect to those of the pure *Pnma* state. Note that recent measurements[36] showed that BFO bulks can exhibit a multidomain consisting of two domains alternating along a ⟨100⟩ direction and for which one domain has a much larger polarization than the other one—exactly as in the multidomain we consider in the present work.

Since all the values reported in Table I for the relaxed multidomain correspond to averages over the modified regions, we also decided to look at the FE/AFE displacements and the oxygen octahedra tiltings along [100] lines crossing the two domains—to better understand how the multidomain locally rearranges itself. These results are displayed in Fig. 2. More precisely, Fig. 2(a) shows the three Cartesian components of the local modes, $\boldsymbol{u}_i$, as a function of the index of Bi ions existing along a specific [100] line. Dashed horizontal lines on the left and right sides of that figure represent the AFE displacement associated with the *pure Pnma* phase and the FE motions existing in the *pure R*3*c* state, respectively. Similarly, Fig. 2(b) displays the *x*, *y*, and *z* components of the $\{\boldsymbol{\omega}_i\}$ vectors as a function of the index of Fe ions present along a [100] line. Dashed horizontal lines in Fig. 2(b) characterize the in-phase and out-of-phase oxygen octahedra tilting occurring in both the nominal *Pnma* and the *R*3*c* states. Note that *anti*ferroelectricity (respectively, *anti*phase tilting) can be easily seen via the change of sign of some components of the local modes (respectively, $\{\boldsymbol{\omega}_i\}$) when going from one Bi site (respectively, Fe site) to its neighboring one along the *x* axis. Figure 2(a) reveals that, in layers 4-9, the *modified Pnma* region has acquired a polarization along the *x* axis that is quite homogeneous, in addition to the AFE displacements (along [011] and $[0\bar{1}\bar{1}]$), which are comparable to those of the pure *Pnma* state. Figure 2(a) further shows that, in layers 13–18 of the modified *R*3*c* region, the component of the polarization along the *x* axis is also homogeneous and is now smaller than its *y* and *z* components—with the latter components being identical to those of the nominal *R*3*c* structure. Note, however, that the *x* component of the polarization in layers 13–18 of the modified *R*3*c* region is still larger (by about twice) than that in layers 4–9 of the modified *Pnma* region, even after relaxation of the multidomain structure. This is likely because the modified *R*3*c* region still needs to have a large *total* polarization without changing its *y* and *z* component. Moreover, Fig. 2(b) reveals that, in layers 4–9 of the modified *Pnma* region, both the in-phase tiltings about the *x* axis and the antiphase tiltings about [110] are similar to those of the pure *Pnma* state. The inside of the modified *R*3*c* region (i.e., layers 13–18) also possesses an antiphase tilting that is very close to that of the pure *R*3*c* state. Due to the aforementioned behaviors of the local modes and oxygen octahedral tiltings, one can therefore consider layers 4–9 of the modified *Pnma* regions and layers 13–18 of the modified *R*3*c* region as being composed of (orthorhombic, polar) $Pna2_1$ and (monoclinic) *Cc* phases, respectively, as a response to the cohabitation between nominal *Pnma* and *R*3*c* states. It is interesting to realize that (pure) $Pna2_1$ has been predicted to be a meta-stable state of BFO bulk[19] and that the *R*3*c* phase of BFO bulk is known to evolve into a *Cc* state in BFO films under epitaxial strains .[37–39]

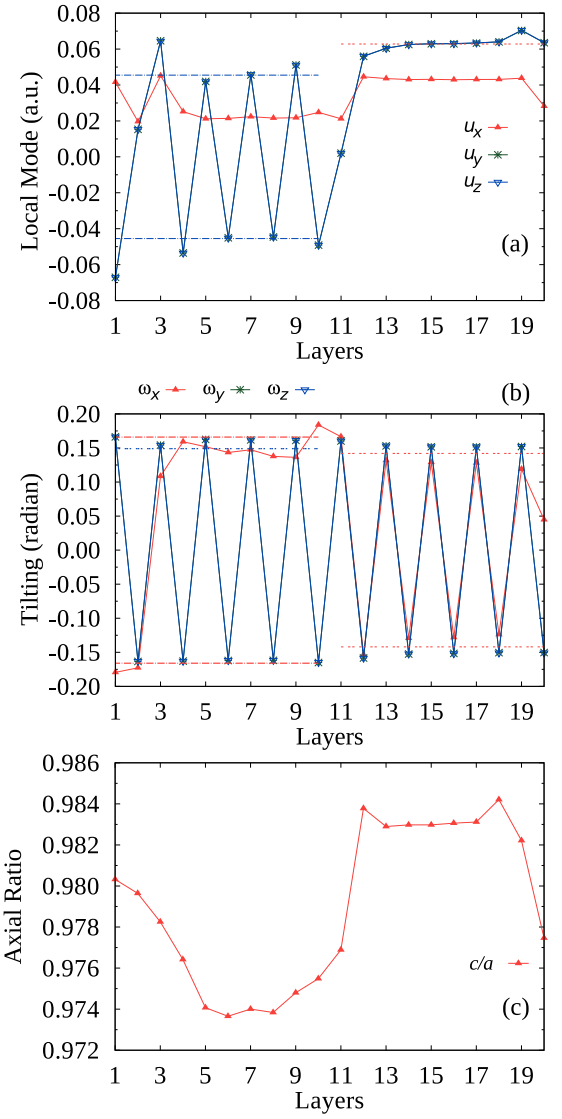

FIG. 2. (Color online) Local modes (a), oxygen octahedral tilting (b), and axial ratio (c) as a function of site index along a [100] line. (a) Horizontal dashed (blue) lines in layers 1 to 10 represent the *y* or *z* component of the antiferroelectric displacements inherent to the pure *Pnma* state, while the horizontal dashed (red) line in layers 11 to 20 is associated with the *x*, *y*, or *z* component of the polarization in the pure *R*3*c* state. (b) The horizontal dashed (blue) line and the horizontal dashed (red) lines in layers 1 to 10 represent the in-phase and antiphase tilting, respectively, of the pure *Pnma* state. The antiphase tilting of the pure *R*3*c* state is also shown by horizontal dashed (red) lines in layers 11 to 20.

Moreover, the studied multidomain configuration generates, after relaxation, its own domain walls, which form at the $R3c/Pnma$ interface (which is made by layers 19 and 20 but also by layers 1–3, because of periodic conditions) and at the $Pnma/R3c$ interface (which is made up of layers 10–12). These layers exhibit structural properties that are neither similar to those of layers 4–9 nor analogous to those of layers 13–18. In particular, layers 1 and 2 have an in-phase tilting about $[\bar{1}00]$ rather than [100], which allows an antiphase rotation about [100] or $[\bar{1}00]$ (in the modified $R3c$ region) to become an in-phase rotation about [100] (in the modified $Pnma$ region). It is also interesting to realize that layers 20, 1, 2, and 3 can be considered as forming a nanoscale twinned phase (this kind of phase has been predicted to be intermediate between $R3c$ and $Pnma$ with an increase in the temperature of the BFO bulk.)[21] As a matter of fact, and similarly to the nanoscale twinned phases described in Ref. 21, these layers (i) possess antiphase oxygen octahedral tilting about [011]; (ii) exhibit complex oxygen octahedral tilting about [100] [namely, counterclockwise for layer 20, clockwise for layer 1, clockwise for layer 2, and then counterclockwise for layer 3, according to Fig. 2(b)]; (iii) have AFE-like displacements along [011] or $[0\bar{1}\bar{1}]$ when going from one (100) to another (100) plane; and (iv) adopt an (inhomogeneous) polarization along the direction about which the oxygen octahedra tilt in a complex fashion (i.e., about [100] here).

Other original features of the domain walls are that (i) the polar y and z displacements nearly vanish at layer 11 [see also the right in Fig. 1(a)], which allows the transition from the AFE pattern of the modified $Pnma$ region to the FE pattern of the modified $R3c$ region to occur via a layer that has only a small polarization along [100]; and (ii) the x component of the polarization significantly "jumps" between layer 11 and layer 12, implying that the dot product between the polarization and the normal of the wall is not fully conserved when crossing the domain wall, as also consistent with recent works.[41–44] Such a deviation from this rule, and the resulting jump of the polarization, may be used to generate a photovoltaic effect.[45]

Moreover, Fig. 2(c) displays the c/a axial ratio (where c is the lattice constant along the domain propagation, which is along the x axis, while a is the lattice constant along the y and z directions) along the [100] line used in Fig. 2(a). Each relaxed domain adopts its own axial ratio, while some walls provide a smooth and continuous evolution of this axial ratio, analogous to the experimental finding in Ref. 14. Interestingly, our simulations further indicate (not shown here) that these changes in c/a are solely due to the fact that the relaxed $Pnma$ and $R3c$ domains, as well as the walls, have different lattice constants along the domain propagation since a is found to be nearly constant throughout the entire multidomain. Note that our axial ratios (which gather inhomogeneous and homogeneous strains) are centered on Bi sites and that, during the simulations, the total energy of the effective Hamiltonian is minimized with respect to all its degrees of freedom (including strains). This implies that our mechanical boundary conditions correspond to zero stress.

Figure 3 also shows that a multidomain made of structurally different domains can have other unusual properties. As a matter of fact, the homogeneous strain η_1 along the domain propagation adopts five successive regions inside which it slightly increases, with these regions being connected by sudden large jumps of the strain, when a continuously increasing electric field is applied along the [111] pseudocubic direction (note that each MC simulation corresponds to an electric field of fixed magnitude and that we let the system relax to equilibrium by using a large number of MC sweeps under this field. We then increase the magnitude of this field from one simulation to another). This striking behavior bears some resemblance to the quantum Hall effect[46] and the Barkhausen effect in ferromagnets.[47] These jumps in strain characterize a sudden large change in the averaged lattice constant along the [100] direction and are therefore associated with anomalously large piezoelectric responses. Each of the four jumps depicted in Fig. 3 was found to correspond to some $Pnma$-like layers transforming into $R3c$-like regions inside the multidomain. Our simulations therefore confirm an hypothesis in Ref. 17, namely, that phase interconversion in an applied electric field can result in large and unusual physical responses. To better understand the origin of the jumps in Fig. 3, let us note that the distribution of local modes shown in Fig. 2(a) implies that an inhomogeneous depolarizing field is built inside the whole system. When an external electric field is applied along [111], the layers in the (modified) $Pnma$ region, where the depolarizing field is the weakest, will be the first layers that transform to $R3c$-like layers. Then, when the external electric field is large enough, other $Pnma$ layers, where the depolarizing field is initially stronger, can finally transform to $R3c$-like layers. As a result, we numerically found that (a) the $Pnma$ layer that first transforms to an $R3c$-like phase is located in the middle of the $Pnma$ region (layer 8 in Fig. 2), and (b) the last two $Pnma$ layers that evolve into an $R3c$ phase are on the domain wall boundary, where the depolarizing field was initially the strongest.

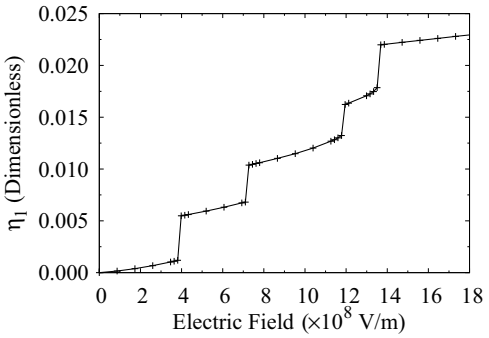

FIG. 3. Homogeneous strain, η_1, along the domain propagation as a function of the magnitude of an electric field applied along the pseudocubic [111] direction. The zero of strain corresponds to the case in which no field is applied.

We now turn our attention to the magnetic properties of the studied multidomain. For that, it is first important to know that the nominal $R3c$ and $Pnma$ states of BFO can have a similar G-type antiferromagnetic vector that lies along the $[01\bar{1}]$ direction. On the other hand, as indicated in Table I, these two states have their own (weak) FM vector, since $\langle \boldsymbol{m} \rangle$ is along the $[2\bar{1}\bar{1}]$ direction in the pure $R3c$ state, while it is along the x axis in the pure $Pnma$ phase. These two canted states are well known in the literature on BFO (for the $R3c$ phase, see Refs 25 and 48 and references therein) and of rare-earth

orthoferrites (for the *Pnma* phase, see, e.g., Ref. 49). It is also interesting to realize that Table I reveals that the pure *Pnma* phase of BFO adopts an FM vector that is larger in magnitude than that of the pure $R3c$ state. The aforementioned difference in direction and magnitude of the weak FM moment between these two phases can be easily understood via the recently discovered law[50] hat directly relates the FM moment to the cross product between the *G*-type antiferromagnetic vector and the $\langle \boldsymbol{\omega}_R \rangle$ antiphase tilting vector. Regarding the magnetic configuration of the multidomain structure, it is found that there is a homogeneous *G*-type antiferromagnetic vector inside the whole system. Moreover, the modified *Pnma* region has an FM vector that is identical in direction and magnitude to that of the pure *Pnma* state (i.e., it lies along [100] and has a magnitude of 0.04 Bohr magneton), while the weak FM vector of the modified $R3c$ region has increased and rotated from the $[2\bar{1}\bar{1}]$ to the $[3\bar{1}\bar{1}]$ pseudocubic direction with respect to that of the pure $R3c$ state. This elongation and rotation occur to make this FM vector more similar to that of the modified *Pnma* region. The studied multidomain configuration can thus also generate novel magnetic behavior.

IV. CONCLUSION

In this work, we have employed a Heff approach to investigate unusual multidomain structures in $BiFeO_3$, finding that a stable multidomain, in which different structural phases coexist and cooperate, can indeed exist. In addition to its complex structural relaxation, done to accommodate the coexistence of these different phases, the multidomain under investigation also shows other interesting properties, such as sudden jumps of the strain under an electric field and other novel magnetic properties. By creating and studying these kinds of multidomains, one may therefore envision a new kind of engineering of structural, magnetic, and physical properties. We thus hope this study will encourage this line of research in several types of materials, e.g., FEs, magnets, and multiferroics.

ACKNOWLEDGMENTS

We thank Dr. Ucko for pointing out the analogy between Fig. 3 and the Barkhausen effect. This work was financially supported by ARO Grant No. W911NF-12-1-0085. L.B. also acknowledges the Department of Energy, Office of Basic Energy Sciences, under Contract No. ER-46612, NSF Grant No. DMR-1066158, and ONR Grant Nos. N00014-11-1-0384 and N00014-12-1-1034 for discussions with scientists sponsored by these grants. D.W. acknowledges support from the National Natural Science Foundation of China under Grant No. 51272204. E.K.H.S. is grateful to the EPSRC for support (Grant No. RG66344). Some computations were also made possible thanks to MRI Grant No. 0722625 from the NSF.

*dawei.wang@mail.xjtu.edu.cn

[1] G. Caatalan, J. Seidel, R. Ramesh, and J. F. Scott, Rev. Mod. Phys. **84**, 119 (2012).
[2] A. Hubert and R. Shafer, *Magnetic Domains* (Springer, New York, 2000).
[3] A. Aird and E. K. H. Salje, J. Phys.: Condens. Matter **10**, 377 (1998).
[4] P. Maksymovych, J. Seidel, Y. Chu, P. Wu, A. P. Baddorf, L. Chen, S. V. Kalinin, and R. Ramesh, Nano Lett. **11**, 1906 (2011).
[5] N. Balke, B. Winchester, W. Ren, Y. Chu, A. N. Morozovska, E. A. Eliseev, M. Huijben, R. K. Vasudevan, P. Maksymovych, J. Britson, S. Jesse, I. Kornev, R. Ramesh, L. Bellaiche, L. Chen, and S. V. Kalinin, Nat. Phys. **8**, 81 (2012).
[6] T. Choi, S. Lee, Y. J. Choi, V. Kiryukhin, and S.-W. Cheong, Science **324**, 63 (2009).
[7] M. Alexe and D. Hesse, Nat. Commun. **2**, 256 (2011).
[8] M. Calleja, M. T. Dove, and E. K. H. Salje, J. Phys.: Condens. Matter **15**, 2301 (2003).
[9] L. Goncalves-Ferreira, S. A. T. Redfern, E. Artacho, and E. K. H. Salje, Phys. Rev. Lett. **101**, 097602 (2008).
[10] S. Van Aert, S. Turner, R. Delville, D. Schryvers, G. Van Tendeloo, and E. K. H. Salje, Adv. Mater. **24**, 523 (2012).
[11] A. N. Morozovska, E. A. Eliseev, M. D. Glinchuk, L. Q. Chen, and V. Gopalan, Phys. Rev. B **85**, 094107 (2012).
[12] E. K. H. Salje, Chem. Phys. Chem. **11**, 940 (2010).
[13] O. Diéguez, P. Aguado-Puente, J. Junquera, and J. Íñiguez, Phys. Rev. B **87**, 024102 (2013).
[14] R. J. Zeches, M. D. Rossell, J. X. Zhang, A. J. Hatt, Q. He, C.-H. Yang, A. Kumar, C. H. Wang, A. Melville, C. Adamo, G. Sheng, Y.-H. Chu, J. F. Ihlefeld, R. Erni, C. Ederer, V. Gopalan, L. Q. Chen, D. G. Schlom, N. A. Spaldin, L. W. Martin, and R. Ramesh, Science **326**, 977 (2009).
[15] Z. Chen, S. Prosandeev, Z. L. Luo, W. Ren, Y. Qi, C. W. Huang, L. You, C. Gao, I. A. Kornev, T. Wu, J. Wang, P. Yang, T. Sritharan, L. Bellaiche, and L. Chen, Phys. Rev. B **84**, 094116 (2011).
[16] M. D. Rossell, R. Erni, M. P. Prange, J.-C. Idrobo, W. Luo, R. J. Zeches, S. T. Pantelides, and R. Ramesh, Phys. Rev. Lett. **108**, 047601 (2012).
[17] J. X. Zhang, B. Xiang, Q. He, J. Seidel, R. J. Zeches, P. Yu, S. Y. Yang, C. H. Wang, Y.-H. Chu, L. W. Martin, A. M. Minor, and R. Ramesh, Nat. Nano. **6**, 98 (2011).
[18] A. Jiang, C. Wang, K. Jin, X. Liu, J. F. Scott, C. Hwang, T. Tang, H. Lu, and G. Yang, Adv. Mater. **23**, 1277 (2011).
[19] O. Diéguez, O. E. González-Vázquez, J. C. Wojdel and J. Iñiguez, Phys. Rev. B **83**, 094105 (2011).
[20] D. C. Arnold, K. S. Knight, F. D. Morrison, and P. Lightfoot, Phys. Rev. Lett. **102**, 027602 (2009).
[21] S. Prosandeev, D. Wang, W. Ren, J. Iñiguez, and L. Bellaiche, Adv. Funct. Mater. **23**, 234 (2013).
[22] L. Bellaiche and J. Íñiguez, Phys. Rev. B **88**, 014104 (2013).
[23] I. A. Kornev, S. Lisenkov, R. Haumont, B. Dkhil, and L. Bellaiche, Phys. Rev. Lett. **99**, 227602 (2007).
[24] S. Lisenkov, I. A. Kornev, and L. Bellaiche, Phys. Rev. B **79**, 012101 (2009); **79**, 219902(E) (2009).
[25] D. Albrecht, S. Lisenkov, W. Ren, D. Rahmedov, I. A. Kornev, and L. Bellaiche, Phys. Rev. B **81**, 140401(R) (2010).
[26] W. Zhong, D. Vanderbilt, and K. M. Rabe, Phys. Rev. Lett **73**, 1861 (1994); Phys. Rev. B **52**, 6301 (1995).

[27]I. A. Kornev, L. Bellaiche, P.-E. Janolin, B. Dkhil, and E. Suard, Phys. Rev. Lett. **97**, 157601 (2006).
[28]J. B. Neaton, C. Ederer, U. V. Waghmare, N. A. Spaldin, and K. M. Rabe, Phys. Rev. B **71**, 014113 (2005).
[29]J. M. Moreau, C. Michel, R. Gerson, and W. J. James, J. Phys. Chem. Solids **32**, 1315 (1971).
[30]F. Kubel and H. Schmid, Acta Crystallogr. B **46**, 698 (1990).
[31]I. Sosnowska, W. Schäfer, W. Kockelmann, K. H. Andersen, and I. O. Troyanchuk, Appl. Phys. A **74**, S1040 (2002).
[32]L. W. Martin, S. P. Crane, Y.-H. Chu, M. B. Holcomb, M. Gajek, M. Huijben, C.-H. Yang, N. Balke, and R. Ramesh, J. Phys.: Condens. Matter **20**, 434220 (2008).
[33]S. K. Streiffer, J. A. Eastman, D. D. Fong, C. Thompson, A. Munkholm, M. V. Ramana Murty, O. Auciello, G. R. Bai, and G. B. Stephenson, Phys. Rev. Lett. **89**, 067601 (2002).
[34]S. K. Streiffer, C. B. Parker, A. E. Romanov, M. J. Lefevre, L. Zhao, J. S. Speck, W. Pompe, C. M. Foster, and G. R. Bai, J. Appl. Phys. **83**, 2742 (1998).
[35]W. Ren, Y. Yang, O. Diéguez, J. Iñiguez, N. Choudhury, and L. Bellaiche, Phys. Rev. Lett. **110**, 187601 (2013).
[36]C. Jia, L. Jin, D. Wang, S. Mi, M. Alexe, D. Hesse, H. Reichlova, X. Marti, L. Bellaiche, and K. W. Urban (unpublished).
[37]I. C. Infante, J. Juraszek, S. Fusil, B. Dupé, P. Gemeiner, O. Diéguez, F. Pailloux, S. Jouen, E. Jacquet, G. Geneste, J. Pacaud, J. Ìñiguez, L. Bellaiche, A. Barthélémy, B. Dkhil, and M. Bibes, Phys. Rev. Lett. **107**, 237601 (2011).
[38]B. Dupé, S. Prosandeev, G. Geneste, B. Dkhil, and L. Bellaiche, Phys. Rev. Lett. **106**, 237601 (2011).
[39]Y. Yang, W. Ren, M. Stengel, X. H. Yan, and L. Bellaiche, Phys. Rev. Lett. **109**, 057602 (2012).
[40]I. Ponomareva, I. I. Naumov, I. Kornev, H. Fu, and L. Bellaiche, Phys. Rev. B **72**, 140102(R) (2005).
[41]B. Meyer and D. Vanderbilt, Phys. Rev. B **65**, 104111 (2002).
[42]J. Hlinka and P. Marton, Phys. Rev. B **74**, 104104 (2006).
[43]M. Taherinejad, D. Vanderbilt, P. Marton, V. Stepkova, and J. Hlinka, Phys. Rev. B **86**, 155138 (2012).
[44]E. A. Eliseev, P. V. Yudin, S. V. Kalinin, N. Setter, A. K. Tagantsev, and A. N. Morozovska, Phys. Rev. B **87**, 054111 (2013).
[45]S. Y. Yang, J. Seidel, S. J. Byrnes, P. Shafer, C.-H. Yang, M. D. Rossell, P. Yu, Y.-H. Chu, J. F. Scott, J. W. Ager, III, L. W. Martin, and R. Ramesh, Nat. Nano. **5**, 143 (2010).
[46]K. V. Klitzing, G. Dorda, and M. Pepper, Phys. Rev. Lett. **45**, 494 (1980).
[47]H. Barkhausen, Physik. Z. **20**, 401 (1919).
[48]C. Ederer and N. A. Spaldin, Phys. Rev. B **71**, 060401 (2005).
[49]L. T. Tsymbal, V. I. Kamenev, Y. B. Bazaliy, D. A. Khara, and P. E. Wigen, Phys. Rev. B **72**, 052413 (2005).
[50]L. Bellaiche, G. Zhigang, and I. Kornev, J. Phys.: Condens. Matter **24**, 312201 (2012).